Quasi-Two-Dimensional Metallic Character of Sm_2Te_5 and $SmTe_3$

E. DiMasi, B. Foran, M. C. Aronson,* and S. Lee*

Departments of Chemistry and Physics, University of Michigan, Ann Arbor, Michigan 48109

Received May 3, 1994. Revised Manuscript Received June 27, 1994®

We demonstrate that the rare-earch polychalcogenides Sm_2Te_5 and $SmTe_3$ are metals and despite optimal Fermi surface nesting contain undistorted tellurium square lattice sheets. Our resistivity measurements reveal an extremely large electrical anisotropy for both Sm polytellurides. Single-crystal X-ray structure refinements of both phases show highly isotropic metallic tellurium atoms. Magnetic susceptibility measurements reveal that the Sm valence is close to 3. For $SmTe_3$ and Sm_2Te_5 the resistivity perpendicular to the plane of the layers is quadratic in temperature, with T^2 coefficients which are 5–6 orders of magnitude larger than those of simple metals. These results firmly establish that the rare-earth polychalcogenides as a family span the metal–insulator boundary.

Introduction

One of the abiding interests in materials chemistry is the synthesis and characterization of new materials that are near the metal–insulator boundary. Such materials exhibit important properties such as high and moderately high-T_c superconductivity (copper oxides, Chevrel phases, and doped fullerenes),[1] commensurate and incommensurate charge density waves (early transition metal chalcogenides and transition metal oxide bronzes),[2] mixed-valence effects (rare-earth monochalcogenides and the Verwey transition of Fe_3O_4),[3] and Mott–Hubbard transitions (as in early transition metal oxides).[4]

In this paper we consider the rare-earth polychalcogenides ZQ_2, Z_2Q_5, and ZQ_3 (Z = rare earth, Q = S, Se, Te), layered materials which exhibit both charge density waves and magnetism.[5] All members of this family are structurally related and have tetragonal or pseudotetragonal symmetry. These structures are based on two motifs, illustrated in the structure of $SmTe_2$ (Figure 1). One motif is a corrugated cubic layer of Sm and Te atoms, while the second is a planar square lattice sheet of chalcogen atoms. In this sheet, the orbitals of the 4-fold coordinated chalcogens are expected to broaden into dispersive bands, allowing metallic behavior.[6] However, Peierls distortions have been observed in the planar chalcogen sheets of some compounds in this family. Some such charge density wave insulators are $LaSe_2$, $Ce_{10}Se_{19}$, $DySe_{1.85}$, and $RbDy_3Se_8$.[7]

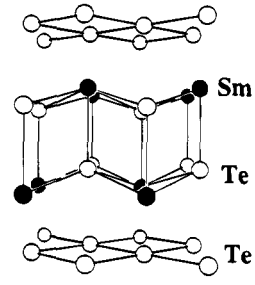

Figure 1. Ball-and-stick representation of $SmTe_2$ (Cu_2Sb) structure type.

Up to now there has been no definitive evidence for undistorted metallic phases in the rare-earth polychalcogenide family. For example, the rare-earth tritelluride $NdTe_3$ has undistorted square sheets of tellurium with each Te atom having four Te–Te bonds of 3.08 Å[8] and would consequently be expected to be metallic. Unfortunately, no resistivity measurements have been reported for $NdTe_3$, the only rare-earth tritelluride for which a single-crystal structure determination had been made. While the existing diffraction results for $LaTe_3$ are insufficiently detailed to determine Te sheet coordination,[9] conductivity measurements reported for pressed powders of $LaTe_3$ indicate that this material is semiconducting.[10] However, even these transport measurements are compromised, since for powder samples intergranular scattering often obscures the intrinsic properties of the crystal. For this reason a clear picture of the transport properties of undistorted rare-earth

* To whom correspondence should be addressed.

® Abstract published in *Advance ACS Abstracts,* August 15, 1994.

(1) (a) Malik, S. K.; Vijayaraghavan, R. *Rev. Solid State Sci.* **1988,** *2,* 75. (b) Chevrel, R.; Sergent, M.; Prigent, J. *J. Solid State Chem.* **1971,** *3,* 515. (c) Hebard, A. F.; Rosseinsky, M. J.; Haddon, R. C.; Murphy, D. W.; Glarum, S. H.; Palstra, T. T. M.; Ramirez, A. P.; Kortan, A. R. *Nature (London)* **1991,** *350,* 600.

(2) (a) Wilson, J. A.; DiSalvo, F. J.; Mahajan, S. *Adv. Phys.* **1975,** *24,* 117. (b) Monceau, P.; Ong, N. P.; Portis, A. M.; Meerschaut, A.; Rouxel, J. *Phys. Rev. Lett.* **1976,** *37,* 602. (c) Rouxel, J.; Schlenker, C. In: *Charge Density Waves in Solids*; Gor'kov, L. P., Grüner, G., Eds.; Elsevier: Amsterdam, 1989.

(3) (a) Jayaraman, A. In: *Handbook on the Physics and Chemistry of Rare Earths*; Gschneider, K. A., Jr., Eyring, L., Eds.; North-Holland Publishing: Amsterdam, 1979; Vol. 2, p 575. (b) Verwey, E. J. W.; Haayman, P. W. *Physics (Utrecht)* **1941,** *8,* 979.

(4) Mott, N. F. *Metal-Insulator Transitions*; Taylor and Francis Ltd.: London, 1974.

(5) Bucher, E.; Andres, K.; DiSalvo, F. J.; Maita, J. P.; Gossard, A. C.; Cooper, A. S.; Hull, G. W., Jr. *Phys. Rev. B* **1975,** *11,* 500 and references therein.

(6) Martin, R. M.; Lucovsky, G.; Helliwell, K. *Phys. Rev. B* **1976,** *13,* 1383.

(7) (a) $LaSe_2$: Bénazeth, S.; Carré, D.; Laruelle, P. *Acta Crystallogr.* **1982,** *B38,* 33. (b) $Pr_{10}Se_{19}$ and $Ce_{10}Se_{19}$: Plambeck-Fischer, P.; Abriel, W.; Urland, W. *J. Solid State Chem.* **1989,** *78,* 164. (c) $DySe_{1.85}$ and $RbDy_3Se_8$: Foran, B.; Lee, S.; Aronson, M. C. *Chem. Mater.* **1993,** *5,* 974.

(8) Norling, B. K.; Steinfink, H. *Inorg. Chem.* **1966,** *5,* 1488.

(9) Ramsey, T. H.; Steinfink, H.; Weiss, E. J. *Inorg. Chem.* **1965,** *4,* 1154.

(10) Ramsey, T. H.; Steinfink, H.; Weiss, E. J. *J. Appl. Phys.* **1965,** *36,* 548.

0897-4756/94/2806-1867$04.50/0

polychalcogenides has awaited the availability of large single crystals. Indeed, although the rare-earth polychalcogenides were first discovered 30 years ago, there was previously no evidence that these compounds are ever metals.

In this paper we present the first evidence for the existence of a metal–insulator boundary in the rare-earth polychalcogenides. Using a flux growth technique, we have prepared large single crystals of Sm_2Te_5 and $SmTe_3$. Electrical resistivity measurements parallel and perpendicular to the layers demonstrate that these materials are quasi-two-dimensional metals. We also reexamine the crystal structures of Sm_2Te_5 and $SmTe_3$. Previous studies of the Z_2Q_5 and ZQ_3 structure types did not rule out the existence of subtle distortions in these compounds. For the Z_2Q_5 structure type, no single crystal study had been reported, as the previous structural solution was based entirely on one powder diffractogram of Nd_2Te_5.[11] In the case of the ZQ_3 structure type the previous single-crystal study of $NdTe_3$ showed strong thermal anisotropies suggestive of the onset of a Peierls distortion.[8] We undertook single-crystal studies of both Sm_2Te_5 and $SmTe_3$. We find that although there are observable distortions and defects in both the $SmTe_3$ and Sm_2Te_5 phases, there exist sheets of tellurium atoms which retain an essentially ideal square symmetry.

Experimental Section

Samples were prepared from stoichiometric mixtures of Sm and Te, with RbCl and LiCl added as flux. All ingredients were obtained from Aldrich with nominal purities of respectively 99.9, 99.999, 99.8, and 99+%. Reaction mixtures were sealed in evacuated quartz tubes and heated to 680 °C for 3 days, then slowly cooled (~0.05 °C/min) to 540 °C before rapid cooling (~3 °C/min) to room temperature. After reaction, tubes were opened and flux was rinsed away with water, ethanol, and finally acetone. Samples were kept under mineral oil or in a glovebox, as these compounds show noticeable change after several days' exposure to air.

X-ray powder patterns were made (Enraf-Nonius Guinier camera, Cu $K\alpha_1$, with NIST Si as an internal standard) and were indexed using the LAZY-PULVERIX program.[12] Electron microprobe analysis was used to determine stoichiometry.[13] Atomic absorption spectroscopy was used to check for incorporation of flux elements. Single crystals were selected using Weissenberg photos to determine crystal quality. Conditions for the X-ray data set collection are included in the supplementary material (see paragraph at end of paper).

Electrical resistivity measurements were performed on single crystals of Sm_2Te_5 and $SmTe_3$ using an ac current source and lockin amplifier. Typical sample size was $1 \times 1 \times 0.03$ mm^3, with the sample thickness determined by scanning electron microscope. Platinum wire leads were attached using silver-filled epoxy to Au pads evaporated onto cleaved surfaces, or to In tabs attached using an ultrasonic soldering iron. Separate samples with leads in the van der Pauw[14] and Montgomery[15] configurations were prepared, and the resistivities parallel and perpendicular to the plane of the layers were determined. Magnetization in fields up to 50 kOe over the temperature range 4.0–350 K was measured using a commercial Quantum Designs SQUID magnetometer. The stoichiometries of samples used for restivity and susceptibility measurements were confirmed by electron microprobe.

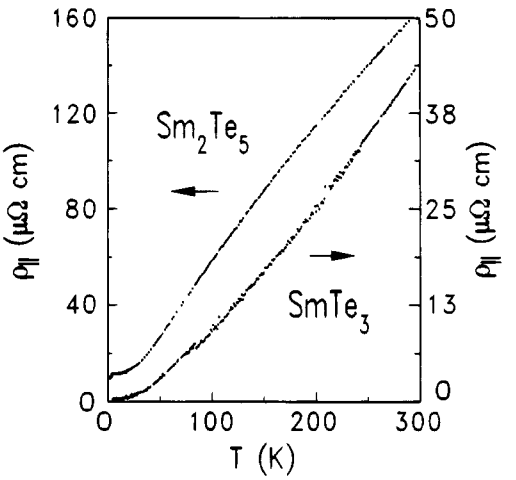

Figure 2. Resistivity $\rho_{||}$ parallel to the layer planes as a function of temperature for Sm_2Te_5 (left axis) and $SmTe_3$ (right axis).

Results

Upon removing the reaction tubes from the furnace, two main products could be distinguished under an optical microscope. Both appeared as shiny metallic-looking crystals, one type orange, the other having a reddish or maroon tint. These color assignments match those of earlier reports for ZQ_3 and Z_2Q_5 phases, respectively.[5] The indexing of Guinier powder patterns for the two main products corresponds closely with previous reports for $SmTe_3$ (orange) and Sm_2Te_5 (red).[5] These stoichiometries were confirmed by electron microprobe analysis. Atomic absorption spectroscopy detected less than 13 μg of Li/g of sample, possibly due to the trapping of lithium salts from the flux between the crystals submitted for analysis. We have also identified a less prevalent product, $SmTe_{2-x}$ ($x \approx 0.0-0.2$), colored similarly to Sm_2Te_5, though darker and harder.

Electrical Resistivity and Magnetic Susceptibility. Electrical resistivity parallel to the layers ($\rho_{||}$) was determined using the van der Pauw method.[14] For these samples, indium contacts span the edge of the sample, electrically shorting the layers so that the current flows essentially parallel to them. Separate samples were prepared having leads in the Montgomery[15] configuration, with sputtered gold contact pads on the surfaces. Measurements on these latter samples were made with current paths both parallel and perpendicular to the layers. Because the resistivity perpendicular to the layers ($\rho_{\perp}$) is much larger than $\rho_{||}$ and because the samples cleave easily, measurements of the current parallel to the layers are particularly susceptible to cracks or inhomogeneities, which would add a perpendicular component to the current path. Such problems are minimized for Montgomery measurements perpendicular to the layers and for the van der Pauw analysis. We combined these two most reliable measurements for the Montgomery analysis, determining $\rho_{\perp}$ using the measured resistance in the perpendicular direction along with the van der Pauw result for $\rho_{||}$.

Figure 2 shows the temperature dependence of the resistivity parallel to the layers over the temperature

(11) Pardo, M.-P.; Flahaut, J. *Bull. Soc. Chim.* **1967**, *10*, 3658.
(12) Yvon, K.; Jeitschko, W.; Parthé, E. *J. Appl. Crystallogr.* **1977**, *10*, 73.
(13) Cameca MBX automated microprobe WDS system with tellurium metal and synthetic samarium garnet of composition $Sm_3Ga_5O_{12}$ as standards. Supported by NSF grant EAR-82-12764.
(14) van der Pauw, L. J. *Philips Res. Rep.* **1958**, *13*, 1.
(15) (a) Montgomery, H. C. *J. Appl. Phys.* **1971**, *42*, 2971. (b) Logan, B. F.; Rice, S. O.; Wick, R. F. *J. Appl. Phys.* **1971**, *42*, 2975.

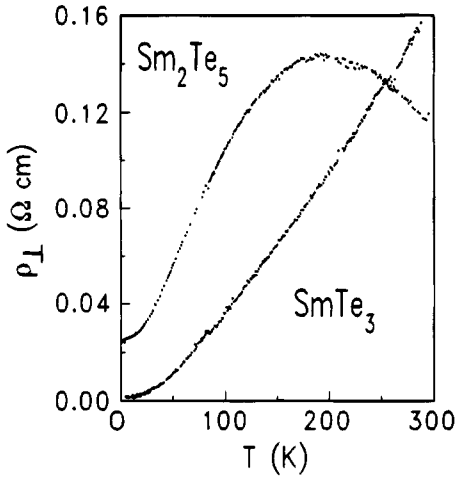

Figure 3. Resistivity $\varrho_\perp$ perpendicular to the layer planes vs temperature for Sm_2Te_5 and $SmTe_3$.

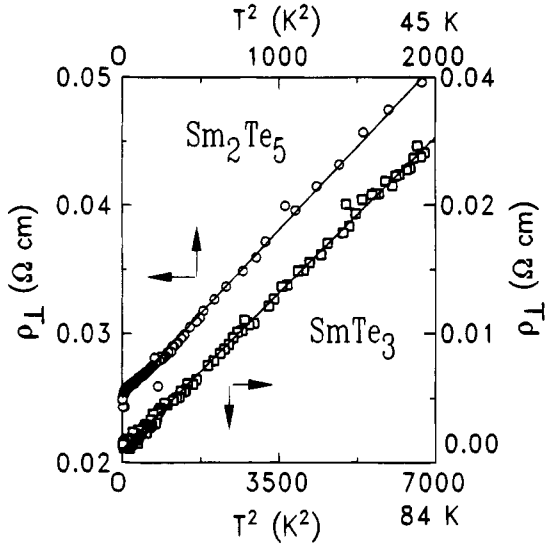

Figure 4. $\varrho_\perp$ plotted against T^2 for Sm_2Te_5 (left and upper axes) and $SmTe_3$ (right and lower axes). Lines are least-squares fits to the data.

range 4.2–300 K for Sm_2Te_5 and $SmTe_3$. For both compounds $\varrho_\parallel$ decreases monotonically with temperature, showing that these materials are metallic. The two compounds differ in the residual resistivity at $T = 0$, which is 20 times larger for Sm_2Te_5. This indicates that disorder plays a larger role in the in-plane transport for Sm_2Te_5 than for $SmTe_3$, in accord with the single-crystal X-ray diffraction results to be described below.

The temperature dependences of $\varrho_\perp$ for Sm_2Te_5 and $SmTe_3$ are shown in Figure 3. For both compounds $\varrho_\perp$ is more than 3 orders of magnitude larger than $\varrho_\parallel$ and follows a T^2 dependence below 45 K for Sm_2Te_5 and below 84 K for $SmTe_3$, as shown in Figure 4. The coefficients of the T^2 term for Sm_2Te_5 and $SmTe_3$ are extremely large, 13.8 μΩ cm K^{-2} and 4.1 μΩ cm K^{-2} respectively, 5–6 orders of magnitude greater than those found for simple metals such as palladium or sodium.[16] At higher temperatures, $\varrho_\perp$ differs notably between $SmTe_3$ and Sm_2Te_5. For $SmTe_3$, $\varrho_\perp$ decreases

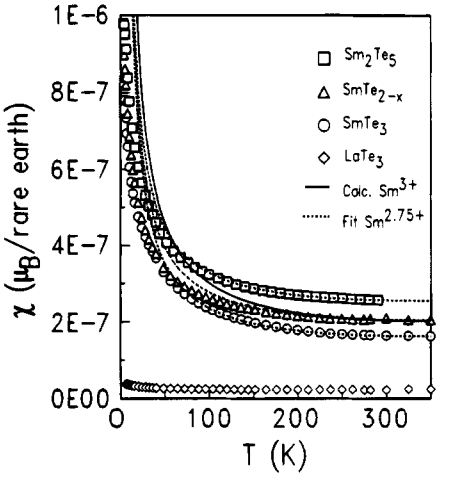

Figure 5. Magnetic susceptibility of Sm_2Te_5, $SmTe_3$, $SmTe_{2-x}$, and $LaTe_3$ vs temperature. The solid line is the calculated paramagnetism for trivalent Sm with spin–orbit splitting of 1500 K.[19] Dashed lines indicate fits as described in text.

monotonically with temperature. By contrast, $\varrho_\perp$ for Sm_2Te_5 initially increases as temperature is decreased, with a broad maximum at ~180 K. The implications of these aspects of the temperature dependence of $\varrho_\perp$ will be addressed below. Like $\varrho_\parallel$, $\varrho_\perp$ has a larger residual value for Sm_2Te_5 than for $SmTe_3$.

We have measured the temperature dependences of the magnetic susceptibilities of Sm_2Te_5, $SmTe_{2-x}$, $SmTe_3$, and $LaTe_3$. The magnetization is linear and nonhysteretic in fields up to 50 kOe. In Figure 5 the susceptibilities χ of all four compounds are shown over the temperature range 4–350 K. A diamagnetic core contribution has been subtracted from all curves.[17] For $LaTe_3$, χ is essentially temperature independent, as expected for a Pauli paramagnet, with a Curie tail indicating small amounts of magnetic impurities. By contrast, the susceptibilities of the Sm compounds are 10 times larger at room temperature than that of $LaTe_3$ and increase substantially at low temperatures, indicating that the magnetic contribution of the Sm atoms has some local character. As a substantial fraction of a free ion moment is associated with Sm^{3+}, while Sm^{2+} is nonmagnetic, these results show that the Sm is not divalent in these materials.

Analysis of our magnetic susceptibility measurements reveals that the Sm valence is close to 3 in the Sm polytellurides. For Sm, the magnetic susceptibility does not follow a Curie–Weiss law, as the effective magnetic moment of the 4f electrons has a temperature dependence arising from low-lying multiplets.[18] In such a system the effective magnetic moment μ_{eff} per rare earth atom can be determined from the measured susceptibility using the relation

$$\mu_{eff} = \sqrt{3\chi k_B T/\mu_B{}^2}$$

where χ is the magnetic susceptibility per atom, k_B is Boltzmann's constant, and μ_B is the Bohr magneton.[18]

The calculated theoretical susceptibility[19] for trivalent Sm with spin–orbit coupling of 1500 K is shown in

(16) (a) Pd: Webb, R. A.; Crabtree, G. W.; Vuillemin, J. J. *Phys. Rev. Lett.* **1979**, *43*, 796. (b) Na: Levy, B.; Sinvani, M.; Greenfield, A. J. *Phys. Rev. Lett.* **1979**, *43*, 1822.

(17) Mulay, L. N.; Boudreaux, E. A. *Theory and Applications of Molecular Diamagnetism*; Wiley: New York, 1976.

(18) Van Vleck, J. H. *The Theory of Electric and Magnetic Susceptibilities*; Oxford (Clarendon Press): London, 1932; pp 239–251.

(19) Frank, A. *Phys. Rev.* **1932**, *39*, 119.

Figure 5 for comparison to the experimental points. For $SmTe_{2-x}$, the data are very close to the theoretical curve above 150 K, while at lower temperatures the susceptibility is reduced from the theoretical value as screening by band electrons becomes increasingly important. Better fits to all three data sets can be obtained by reducing the Sm valence to 2.75 and adding temperature-independent terms which can be interpreted as Pauli paramagnetic contributions. However, such a detailed analysis to determine the valence is probably not warranted, as anomalous temperature dependences of the magnetic susceptibility have been observed in some Sm intermetallics[3a] and as possible crystal field effects and intermoment interactions have not been accounted for.

The evolution of crystal cell parameters across the lanthanide series corroborates the result from magnetic susceptibility that the Sm valence is near 3. Bucher's[5] plot of the lattice constants of the rare earth and La monochalcogenides is compared to those of the layered polychalcogenides in Figure 6. The anomalies at Eu, Sm, Yb, and Tm, indicating rare-earth divalency in the monochalcogenides, are not observed for Sm in the ZTe_3 and Z_2Te_5 phases, which magnetic susceptibility measurements found to be essentially trivalent. We further observe that Eu and Yb polytellurides do not exist in this structural type, emphasizing that divalent rare-earth character is not compatible with the high Te coordination of the rare earth in these structures.

In summary, our transport measurements show that Sm_2Te_5 and $SmTe_3$ are highly anisotropic metals, with low resistivity $\varrho_{\parallel}$ parallel to the plane of the layers, consistent with undistorted Te square sheets. The much larger across-plane resistivity $\varrho_{\perp}$ is characterized at low temperatures by very large T^2 coefficients and in the case of Sm_2Te_5 by a broad resistivity maximum. Our measurements of the magnetic susceptibility indicate that the Sm valence is close to 3 for all three Sm polytellurides.

Structure Determination of $SmTe_3$. A crystal with dimensions of $0.25(1) \times 0.20(1) \times 0.03(1)$ mm^3, with a strong coherent diffraction pattern (Weissenberg photos) was chosen for data set collection (Table 1). Weissenberg photographs showed no superlattice diffraction. We used the original literature report for $NdTe_3$ of Norling and Steinfink[8] as a starting point for our refinement. With isotropic thermal parameters for all atoms, we found $R = 4.33\%$, $R_w = 3.53\%$ for 880 reflections and 10 parameters. The addition of anisotropic thermal parameters for all atoms gave $R = 4.27\%$, $R_w = 3.42\%$ for 880 reflections and 18 parameters. All thermal ellipsoids are nearly spherical. The anisotropic thermal factors originally reported for $NdTe_3$ are probably due to the lack of absorption corrections.

Two large peaks remained in the Fourier difference map with heights of 13.8 and 11.4 e$^-$/Å^3. These residual peaks correspond to a shift of the Sm and Te(1) positions by a vector $(1/2,0,1/2)$ as diagrammed in Figure 7, suggestive of a slip fault. These new atom positions were added to the solution. As these peaks lie only 2 Å away from other rare earth and tellurium positions, we constrained the overall occupations of the original Sm and Te(1) positions together with the new positions to add to a fixed value of 100%. Thus the solution only allowed for variation of occupation between the original

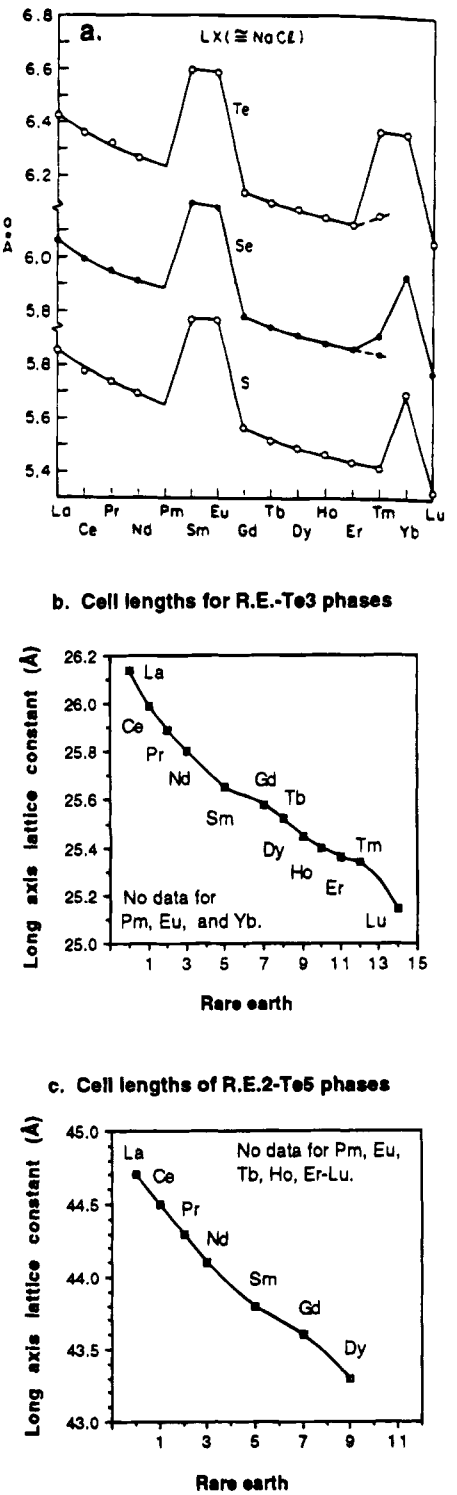

Figure 6. Lattice constants across the lanthanide series. (a) In the rare-earth monochalcogenides anomalies at Sm, Eu, Tm, and Yb indicate divalency (figure from ref 5). For the ZTe_3 (b) and Z_2Te_5 (c) phases, no anomaly at Sm is evident. (Lattice constants for phases other than the Sm polytellurides from ref 29.)

Sm and Te(1) positions and the new slip-fault positions. This solution refined to give an occupation of the slip-fault layer of 3.5% with $R = 3.06\%$, $R_w = 2.29\%$, 880 reflections, and 19 parameters. Final atomic coordinates, thermal factors and occupation factors are reported in Table 2. Interatomic distances are reported in Table 3.

Table 1. Crystallographic Data for $SmTe_3$ and Sm_2Te_5[a]

empirical formula	$SmTe_3$	Sm_2Te_5
crystal color, habit	orange-metallic	purple/red-metallic
crystal size (mm)	0.25(1) × 0.20(1) × 0.03(1)	0.20(1) × 0.20(1) × 0.05(1)
space group	*Cmcm*	*Cmcm*
Z	4	4
a (Å), Guinier/single crystal:	4.341(1)/4.3425(5)	4.3551(7)/4.3620(6)
b (Å)	25.73(2)/25.712(6)	43.64(2)/43.64(1)
c (Å)	4.335(2)/4.3362(5)	4.3551(7)/4.3620(6)
volume (Å^3)	482.8	827.7
density (calc) (g cm^{-3})	7.31	7.42
F(000) (electrons)	1744.0	3072.0
linear abs coeff μ (cm^{-1}):	597.0	625.0
no. of data collected:	11,161	13,447
no. of unique reflections	880 (*Cmcm* allowed)	949
R_{int}	0.0199	0.0572
abs correction from PSI Scans, using Siemen's XEMP, laminar scheme		
principle face	0 1 0	0 1 0
R_{merge} before/after correction	0.2559/0.0459	0.3242/0.0928 = 20
max/min transmission	0.736/0.091	0.478/0.075
refined reflns (F_o) > 0.6$\sigma(F)$	880	949
no. of param refined	18	30
data/parameter ratio:	48.9	31.6
$R = \Sigma(\|F_o - F_c\|)/\Sigma(\|F_o\|)$	0.0304	0.0483
$R_w = [\Sigma(w\|F_o - F_c\|)^2/\Sigma w(F_o)^2]^{1/2}$	0.0229	0.0402
weighting scheme:	$w^{-1} = \sigma^2(F_o)$	$w^{-1} = \sigma^2(F_o)$
goodness of fit	6.047	8.7381
mean shift/error	0.0014	0.0001
max shift/error	0.007	0.001
secondary extinction	1.5 × 10^{-6}	3.2 × 10^{-6}
residual electron density (e$^-$/Å^3)	4.8 and −5.65	4.0 and −3.3

[a] Data were collected on a Siemens upgraded P2$_1$, with Mo Kα = 0.710 73 Å, graphite monochromated, Lp corrected, 23 °C, by $\omega/2\theta$ scans (at 3−6°/min and a scan width from 0.8° below Kα$_1$ to 0.8° above Kα$_2$, with a background/scan ratio of 0.5) for $SmTe_3$. Wyckoff scans (at 4−8°/min) were used for Sm_2Te_5 to avoid possible overlap of scans that could result from the long b axis. Both data sets were collected full sphere, from 5 to 65° in 2θ for $SmTe_3$, and 5 to 80° for Sm_2Te_5. Three standard reflections were measured after every 97, showing less than 2% variation in intensity. Data were processed, and refinement based on Full-matrix-least-squares (function minimized was $w|F_o - F_c|^2$), all using Siemens' SHELXTL PLUS software package on a VAXStation 3500.

Table 2. Atomic Positions and Thermal Factors for $SmTe_3$[a]

atom	*X/A*	*Y/B*	*Z/C*	occupancy	U_{11}	U_{22}	U_{33}	U_{eq}
Sm(1)	0.000 00	0.169 44 (2)	0.250 00	0.964 (1)	0.0093 (1)	0.0095 (2)	0.0097 (2)	0.0095 (1)
Te(1)	0.000 00	0.295 26 (2)	0.250 00	0.964 (1)	0.0090 (2)	0.0089 (2)	0.0094 (2)	0.0091 (1)
Te(2)	0.000 00	0.929 20 (2)	0.250 00	1.000 00	0.0147 (2)	0.0124 (2)	0.0125 (2)	0.0132 (1)
Te(3)	0.000 00	0.570 94 (2)	0.250 00	1.000 00	0.0140 (2)	0.0120 (2)	0.0127 (2)	0.0129 (1)
Sm(2)	0.500 00	0.169 44 (2)	0.750 00	0.036 (1)	0.0094 (1)	0.0095 (2)	0.0097 (2)	0.0095 (1)
Te(4)	0.500 00	0.295 26 (2)	0.750 00	0.036 (1)	0.0094 (1)	0.0095 (2)	0.0097 (2)	0.0095 (1)

[a] For all atoms $U_{12} = U_{23} = U_{13} = 0$. The form of the thermal ellipsoid is $g_i = f_i \exp[-2\pi^2(U_{11}h^2a^{*2} + U_{22}k^2b^{*2} + U_{33}l^2c^{*2} + 2U_{12}hka^*b^* + 2U_{23}klb^*c^* + U_{13}hla^*c^*)]$.

Table 3. Selected Interatomic Distances (Å) for $SmTe_3$

Sm(1)−1 Te(1)	3.233(1)
Sm(1)−4 Te(1)	3.196(1)
Sm(1)−2 Te(2)	3.336(1)
Sm(1)−2 Te(3)	3.332(1)
Te(2)−4 Te(3)	3.065(1)
Sm(2)−2 Te(2)	3.334(1)
Sm(2)−1 Te(4)	3.233(1)
Sm(2)−4 Te(4)	3.196(1)

While the final solution of the structure broadly agrees with that previously reported, we have identified two new pieces of information. First, thermal parameters of Sm and Te(1) are spherical, while square-sheet tellurium atoms show only slight anisotropy. Second, we observe that $SmTe_3$ crystals have a propensity for slip-fault disorder between layers.

Structure Determination of Sm_2Te_5. The crystal selected for data collection was a red square platelet of dimensions 0.20(1) × 0.20(1) × 0.05(1) mm^3. Weissenberg photographs of this crystal revealed an orthorhombic cell with the main diffraction spots showing C-centering systematic extinctions (*hkl*; $h + k$ = odd). However weaker diffraction spots breaking this law were also observed. We collected the full sphere of reflections for the P-type cell. In solving the structure we considered first the C-centered data only. The merging R_{int} for space group *Cmcm* was 5.7%. We used the isotropic solution of Pardo and Flahaut[11] as a starting point for our refinement. Although this earlier study was based on Nd_2Te_5 and involved only 20 diffraction lines from a powder diffractogram, of a then new structure type, the atomic coordinates of this earlier study proved to be remarkably accurate. With our data the structure refined to give R = 4.83%, R_w = 4.02% for 949 unique reflections and 31 parameters. The largest remaining peak in the Fourier difference map was 4.0 e^{-1}/Å^3. Atomic coordinates, occupation and thermal factors are given in Table 4. Interatomic distances are reported in Table 5. An illustration of the structure is given in Figure 8. Only site Te(5) showed either pronounced anisotropy in its thermal factors or significant deviations from full occupation. R_w was minimized when Te(5) was 87.6% occupied with a flattened thermal ellipsoid. In final stages of the refinement occupation on all other atoms varied from full by less than 1.5% (1 esd).

Table 4. Atomic Positions and Thermal Factors for Sm_2Te_5[a]

atom	X/A	Y/B	Z/C	occupancy	U_{11}	U_{22}	U_{33}	U_{eq}
Sm(1)	0.000 00	0.901 16 (3)	0.250 00	1.000 00	0.0135 (4)	0.0120 (7)	0.0111 (4)	0.0122 (3)
Sm(2)	0.000 00	0.693 37 (3)	0.250 00	1.000 00	0.0142 (4)	0.0165 (7)	0.0125 (4)	0.0144 (3)
Te(1)	0.000 00	0.826 42 (3)	0.250 00	1.000 00	0.0134 (5)	0.0129 (8)	0.0120 (4)	0.0127 (4)
Te(2)	0.000 00	0.620 08 (3)	0.250 00	1.000 00	0.0134 (5)	0.0123 (8)	0.0117 (5)	0.0124 (4)
Te(3)	0.000 00	0.458 40 (4)	0.250 00	1.000 00	0.0192 (5)	0.0142 (8)	0.0143 (5)	0.0159 (4)
Te(4)	0.000 00	0.041 51 (4)	0.250 00	1.000 00	0.0202 (5)	0.0139 (9)	0.0138 (5)	0.0160 (4)
Te(5)	0.000 00	0.250 00	0.250 00	0.875 (7)	0.035 (1)	0.010 (1)	0.037 (1)	0.0279 (6)

[a] For all atoms $U_{12} = U_{23} = U_{13} = 0$. The form of the thermal ellipsoid is $g_i = f_i \exp[-2\pi^2(U_{11}h^2a^{*2} + U_{22}k^2b^{*2} + U_{33}l^2c^{*2} + 2U_{12}hka^*b^* + 2U_{23}klb^*c^* + U_{13}hla^*c^*)]$.

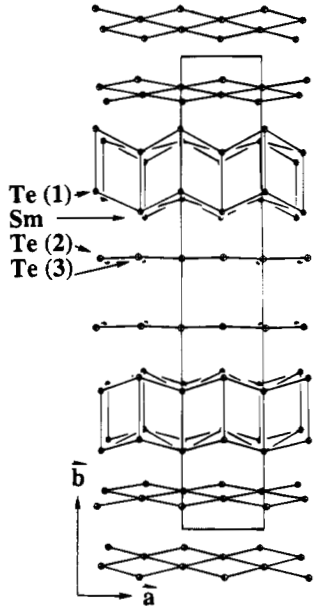

Figure 7. $SmTe_3$ crystal structure showing 50% probability thermal ellipsoids.

Table 5. Interatomic Distances (Å) for Sm_2Te_5

Sm(1)−1 Te(1)	3.262(2)
Sm(1)−4 Te(2)	3.221(1)
Sm(1)−2 Te(3)	3.316(2)
Sm(1)−2 Te(4)	3.319(2)
Sm(2)−1 Te(2)	3.198(2)
Sm(2)−4 Te(1)	3.203(1)
Sm(2)−4 Te(5)	3.296(1)
Te(3)−4 Te(4)	3.084(1)
Te(5)−4 Te(5)	3.084(2)

Although a number of non-C-centered reflections had significant intensities, they were generally of poor quality, with abnormal peak profiles that were not well centered with respect to the orientation matrix of the C-centered data. Attempts to refine the solution in lower space groups did not lead to significant changes in the structure.

In summary, our structure work confirms and elaborates upon the reported structures of the ZQ_3 and Z_2Q_5 phases. As a comparison of Figures 1 and 7 shows, the $SmTe_3$ structure is similar to that of $SmTe_2$ where the single Te square sheets have been replaced by double Te sheets. The Sm_2Te_5 structure may be viewed as an intergrowth of the $SmTe_2$ and $SmTe_3$ structures with alternating single and double Te square sheets interspersed throughout the structure. In Sm_2Te_5, the single-layer-thick tellurium sheets are tellurium deficient with anisotropic thermal parameters indicative of incipient distortions. The lack of superstructure reflections (beyond the doubling of the primitive cell if the non-C-centered reflections are included) rules out the complete ordering of vacancy sites in Sm_2Te_5. This is compatible with the disorder indicated by the increased residual resistivity for Sm_2Te_5 relative to that of $SmTe_3$. Our single-crystal work provides us with a finer view of the distortions and defects which occur in these structures. There is no crystallographic evidence for the onset of a charge density wave in the double tellurium layers, while the single sheets appear to be very close to a structural instability.

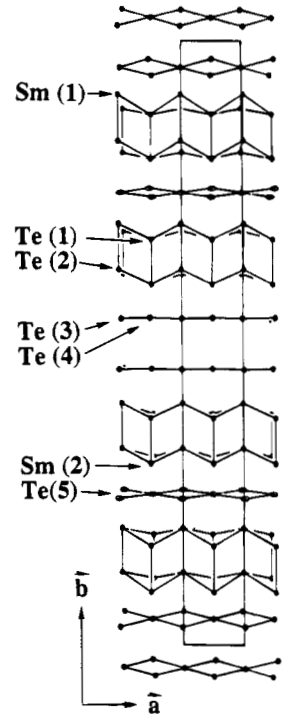

Figure 8. Sm_2Te_5 crystal structure showing 50% probability thermal ellipsoids.

Discussion

The layered structures of the Sm polytellurides readily suggest the possibility that the electrical resistivity should also be anisotropic. The electrical anisotropy $\varrho_\perp/\varrho_\parallel$ is very large at all temperatures, as illustrated in Figure 9, suggesting that charge carriers are largely localized in one of the two types of layers. As $\varrho_\perp$ and $\varrho_\parallel$ are both metallic, we conclude that there are no insulating sheets. We propose a model for the conduction, identifying the contribution of each layer type to the resistivity.

At room temperature $\varrho_\parallel$ is comparable to the resistivity of metallic elemental Te at 200 kbar, ~150 $\mu\Omega$ cm.[20]

(20) Bundy, F. P.; Dunn, K. J. *Phys. Rev. B* **1980**, *22*, 3157.

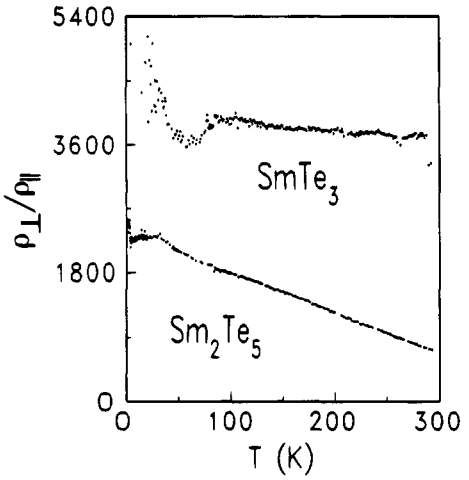

Figure 9. Electrical anisotropy $\varrho_\perp/\varrho_\parallel$ as a function of temperature for both Sm polytellurides.

Table 6. Coefficient *A* of Quadratic Temperature Term in the Electrical Resistivity for Sm Polytellurides, Heavy Fermion Intermetallics, and Simple Free Electron-like Metals

material	A ($\mu\Omega$ cm K^{-2})	ref
$CeAl_3$	35	28a
Sm_2Te_5	13.8	
$CeCu_2Si_2$	10.7	28b
$SmTe_3$	4.1	
SmB_6 (62 kbar)	0.6	23a
UPt_3	0.5	28c
URu_2Si_2	0.17	28d
UAl_2	0.053	28e
Pd	6.4×10^{-5}	16a
Na	1.9×10^{-7}	16b

In both $SmTe_3$ and Sm_2Te_5 the double Te sheets have essentially perfect square symmetry, with no thermal anisotropy to signal an incipient distortion mode. Tight-binding band calculations make clear that in the absence of distortions in the square lattice sheets, these materials should be metallic.[21] The partially occupied band in these calculations is primarily of tellurium 5p character. We conclude that the metallic character of $\varrho_\parallel$ is primarily due to conduction through the undistorted double Te sheets.

For Sm_2Te_5 and $SmTe_3$, $\varrho_\perp = \varrho_0 + AT^2$ at low temperatures. The coefficient A is extremely large for the Sm polytellurides, as shown by the comparison to the quadratic terms of other materials in Table 6. For $SmTe_3$ and Sm_2Te_5 the coefficients A are 5–6 orders of magnitude larger than those found for simple free-electron metals. Such large T^2 dependences have been observed previously only for a small group of rare earth and actinide intermetallics.[22] In these systems, generally referred to as heavy fermions, the enhancement of the T^2 coefficient is understood to result from strong interactions between the magnetic f electrons and the conduction band. The maximum in $\varrho_\perp$ for Sm_2Te_5 is evocative of these heavy fermions and, in particular, of Sm intermetallics such as SmB_6 under pressure.[23] For these well-known systems, the presence of the resistivity maximum reflects correlations between the conduction electrons and the 4f states. By analogy we expect that the resistivity perpendicular to the layers in Sm_2Te_5 and $SmTe_3$ is dominated by such magnetic scattering.

Table 7. Electrical Anisotropies of Sm Polytellurides, Layered Transition Metal Dichalcogenides, and Copper Oxide Superconductors

material	$\varrho_\perp/\varrho_\parallel$ at 4.2 K	ref
$NbSe_2$[a]	7 (31)	30a
1T–TaS_2[a]	500	30b
4Hb–TaS_2[a]	1000	30c
Sm_2Te_5	2200	
$SmTe_3$	5000	
2H–NbS_2	7200	30d
$Bi_{2+x}Sr_{2-y}CuO_{6\pm\delta}$, $Bi_2Sr_{2.2}Ca_{0.8}Cu_2O_8$	40 000–200 000	30e

[a] CDW hosts. Anisotropy at temperatures above the CDW transition given in parentheses for $NbSe_2$.

The electrical anisotropies of the Sm polytellurides are larger than those of many well known layered compounds, as shown in Table 7. A number of these layered systems host charge density waves.[2] For such materials, the high electrical anisotropy enhances the Fermi surface nesting, stabilizing the CDW distortion.[24] Yet our resistivity measurements show no sign of a CDW state for Sm_2Te_5 and $SmTe_3$ from room temperature to 4.2 K. We must caution that except in the case of 2H–$NbSe_2$, the CDW hosts in Table 7 are already in the distorted state at the temperatures for which electrical anisotropy measurements were made, and a complete comparison must await resistivity measurements above the CDW transition temperatures for these systems. Nevertheless, the lack of charge density waves in the Sm polytellurides is startling, considering their high anisotropy as well as the fact that most of the reported rare earth polychalcogenide phases exhibit distorted chalcogen sheets.

There are other factors besides nesting which control the stability of the CDW versus the undistorted metallic state. To delineate these factors, it is useful to discuss the Sm polytellurides within the context of other layered rare earth, alkali, and alkaline earth polychalcogenides. Unfortunately, electrical conductivity and bandgap measurements have yet to be made on many of these polychalcogenides. We therefore turn to structural information to infer the proximity of a given material to the metallic state. We wish to construct a measure of the distortion which can be considered an order parameter for the metal–insulator transition. In particular, we consider the average first nearest neighbor and the shortest second nearest neighbor chalcogen–chalcogen distances. The first nearest neighbors are those chalcogens which need to be considered as bonds in order to fulfill the octet rule requirements of the system. The second nearest-neighbor distance is the next shortest chalcogen–chalcogen distance not required by the octet rule of bonding. We call the average first and second neighbor distances r and s, respectively, and define the departure from metallicity $q = 1 - r/s$. The parameter q has the form of an order parameter: in particular if $q = 0$, the material should be metallic. Conversely for $q > 0$, the system can be assumed to be

(21) Tremmel, W.; Hoffman, R. *J. Am. Chem. Soc.* **1987**, *109*, 124.
(22) Fisk, Z.; Hess, D. W.; Pethick, C. J.; Pines, D.; Smith, J. L.; Thompson, J. D.; Willis, J. O. *Science* **1988**, *239*, 33.
(23) (a) Cooley, J. C. to be published. (b) Berman, I. V.; Brandt, N. B.; Moshchalkov, V. V.; Pashkevich, S. N.; Sidorov, V. I.; Konovalova, E. S.; Paderno, Yu. B. *JETP Lett.* **1983**, *38*, 477. (c) Holtzberg, F.; Wittig, J. *Solid State Commun.* **1981**, *40*, 315.
(24) Whangbo, M.-H.; Canadell, E.; Foury, P.; Pouget, J.-P. *Science* **1991**, *252*, 96.

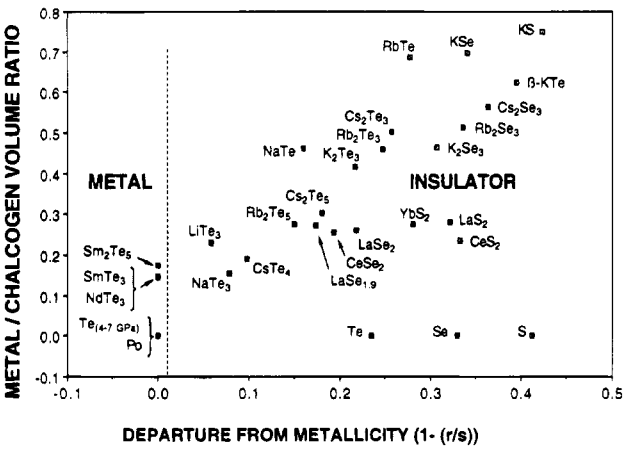

Figure 10. Plot of departure from metallicity vs metal/chalcogen volume ratio.

an insulator. In Figure 10 we plot the volume ratios of the electropositive metal atoms to the chalcogen atoms as a function of q. For these ratios we use the ionic radii of the atoms.[25] For the sake of simplicity we use only one size radius for each chalcogen atom regardless of its formal oxidation state. This figure demonstrates the importance of atomic size in controlling the second-nearest-neighbor contacts. Since large or numerous electropositive cations break the contacts between the chalcogen atoms, metallic character is enhanced in those materials where the electropositive atoms are few or small. As Figure 10 shows, $SmTe_3$ and Sm_2Te_5 have rather low metal/tellurium volume ratios. From a consideration of size factors alone, it is reasonable that $SmTe_3$ and Sm_2Te_5 are metals.

However, size factors alone do not determine whether a material is metallic. Other principle factors are polarizability and electron concentration. Polarizable atoms have a greater propensity for the metallic state.[26] In Figure 10, the more polarizable tellurides are consistently more metallic than their selenide counterparts. This argument can presumably be extended to effects of electron concentration on the polarizability of the tellurium atoms. It is known that negatively charged anions have greater polarizability than their neutral counterparts. We may further expect that the presence of the Sm, by increasing the net negative charge on the tellurium atoms in $SmTe_3$ and Sm_2Te_5, helps drive the systems to the metallic state.

Earlier studies have shown that second-moment-scaled tight-binding theory can be used to evaluate the energies of structures across the metal–insulator transition.[27] In particular, these studies have shown that for electron-rich systems, metallic vs insulating character is caused by a competition between the stability of squares of bonded atoms and bond-breaking distortions.[27] The former leads to metallic character while the latter leads to the semiconducting state.

Two competing effects are observed in band theory calculations. First, as the tellurium atoms become increasingly anionic, the valence p orbitals expand. This expansion, modeled by a decrease in the ζ coefficient for Slater type orbitals, has been shown to have the effect of stabilizing the square lattice and hence the metallic state. However, the increased anionic character of the Te atoms occurs with a simultaneous increase in the percent band filling of the Te p band. Thus a second, competing effect in band calculations is that such an increase in band filling favors the insulating state. The band model suggests that at a certain critical electron concentration a transition will occur from the metallic to the insulating state.[27]

For the Sm polytellurides discussed in this paper, both the polarizability and the size arguments predict the metallic behavior which we observed through electrical resistivity measurements. The band theory arguments suggest that for electron-rich chalcogen sheets, the metallic state is stabilized unless a critical electron concentration is reached. These band theory arguments may be applied specifically to the two different types of Te sheet identified in the Sm polytellurides. While the electron concentration in the double Te sheets allows the metallic state, the more electron-rich single sheet Te sites show thermal anisotropy indicative of distortions that may be associated with loss of metallic character. We conclude that Sm_2Te_5 and $SmTe_3$ do not have sufficiently high electron concentrations in their Te sheets to be insulators. Further studies of more electron rich polytelluride phases would provide an excellent test of this description of charge density wave stability.

Acknowledgment. The authors are grateful for the assistance of Carl Henderson of the University of Michigan Electron Microbeam Analysis Laboratory, Dr. Jeff Kampf of the University of Michigan Chemistry Department, for collection and discussion of single-crystal X-ray data sets, and Mr. N. H. Magida of Thermosen, Inc., for providing special low-level relays used for transport measurements. Acknowledgment is made to the donors of The Petroleum Research Fund, administered by the American Chemical Society, for partial support of this research (E.D. and M.C.A.). We thank the A. P. Sloan Foundation and the J. D. and C. T. MacArthur foundations for fellowships granted to S.L. This research was supported by the National Science Foundation under Grant DMR-9319196.

Supplementary Material Available: Listings of observed and calculated crystal structure factors for $SmTe_3$ and Sm_2Te_5 (8 pages). Ordering information is given on any current masthead page.

(25) Shannon, R. D. *Acta Crystallogr.* **1976**, *A32*, 751.
(26) Edwards, P. P.; Sienko, M. J. *J. Chem. Educ.* **1983**, *60*, 691.
(27) (a) Lee, S.; Foran, B. *J. Am. Chem. Soc.* **1994**, *116*, 154. (b) Lee, S.; Rousseau, R.; Wells, C. *Phys. Rev. B* **1992**, *46*, 12121.
(28) (a) $CeAl_3$: Andres, K.; Graebner, J. E.; Ott, H. R. *Phys. Rev. Lett.* **1975**, *35*, 1779. (b) $CeCu_2Si_2$: Steglich, F.; Bredl, C. D.; Lieke, W.; Rauchschwalbe, U.; Sparn, G. *Physica* **1984**, *126B*, 82. (c) UPt_3: Willis, J. O.; Thompson, J. D.; Fisk, Z.; de Visser, A.; Franse, J. J. M.; Menovsky, A. *Phys. Rev. B* **1985**, *31*, 1654. (d) URu_2Si_2: Palstra, T. T. M.; Menovsky, A. A.; Nieuwenhuys, G. J.; Mydosh, J. A. *J. Magn. Magn. Mater.* **1986**, *54*, 435. (e) UAl_2: Wire, M. S. Thesis, University of California, San Diego, 1984.
(29) Villars, P.; Calvert, L. D. *Pearson's Handbook of Crystallographic Data for Intermetallic Phases*; A.S.M.: Metals Park, OH, 1991.
(30) (a) 2H-$NbSe_2$: Edwards, J.; Frindt, R. F. *J. Phys. Chem. Solids* **1971**, *32*, 2217. Moncton, D. E.; Axe, J. D.; DiSalvo, F. J. *Phys. Rev. B* **1977**, *16*, 801. (b) 1T-TaS_2: Hambourger, P. D.; DiSalvo, F. J. *Physica* **1980**, *99B*, 173. (c) 4Hb-TaS_2: DiSalvo, F. J.; Bagley, B. G.; Voorhoeve, J. M.; Waszczak, J. V. *J. Phys. Chem. Solids* **1973**, *34*, 1357. Wattamaniuk, W. J.; Tidman, J. P.; Frindt, R. F. *Phys. Rev. Lett.* **1975**, *35*, 62. (d) 2H-NbS_2: Pfalzgraf, B. W.; Spreckels, H. *J. Phys. C: Solid State Phys.* **1987**, *20*, 4359. (e) Bi–Sr–Cu–O compounds: Martin, S.; Fiory, A. T.; Fleming, R. M.; Schneemeyer, L. F.; Waszczak, J. V. *Phys. Rev. B* **1990**, *41*, 846.